JOURNAL OF APPLIED ELECTROCHEMISTRY 19 (1989) 856–867

Laminar radial flow electrochemical reactors. III. Electroorganic synthesis

F. B. THOMAS

Hycal Energy Research Labs, 1338A 36th Ave. N.E., Calgary, Alberta, Canada T2E 6T6

P. A. RAMACHANDRAN, M. P. DUDUKOVIC

Chemical Reaction Engineering Laboratory, Washington University, St. Louis, MO 63130, USA

R. E. W. JANSSON

Monsanto Corporation, 800 N. Lindbergh Avenue, St. Louis, MO 63147, USA

Received 3 May 1988; revised 27 June 1988

This paper investigates the performance and design of three laminar radial flow electrochemical cells (the capillary gap cell, stationary discs; the rotating electrolyzer, co-rotational discs; the pump cell, one disc rotating and the other stationary). Modeling of a competing electrosynthesis pathway is described – the methoxylation of furan. The model developed incorporates convective, diffusive and migrative influences with three homogeneous and two electrodic reactions. Two sizes of reactors are considered and the performance of the different reactor types analyzed as a function of size. The superiority of the rotational cells is illustrated for this reaction scheme compared to both the capillary gap cell (CG) and a parallel plate reactor (PPER). Scale-up criteria are scrutinized and two approaches to laminar radial flow reactor scale-up are investigated. The one suggested herein shows that Taylor number, residence time, *IR* drop and rotational Reynolds number must all be accounted for even with a fairly simple electrosynthesis pathway. A quantitative evaluation of this scale-up procedure is included.

Nomenclature

a	gap width (m)
C	dimensionless concentration
D	diffusion coefficient ($m^2 s^{-1}$)
Pe	Peclet number ($v_c a/D$)
Q	volumetric flow rate ($m^3 s^{-1}$)
r	dimensionless radius
R	radius (m)
Re	Reynolds number ($v_c a/\nu$)
Re_θ	rotational Reynolds number ($\omega R_0^2/\nu$)
t	time (s)
τ	residence time of reactor
v_r	dimensionless radial velocity
v_z	dimensionless axial velocity
V	volume (m^3), velocity ($m s^{-1}$) and voltage
z	dimensionless axial distance

Greek symbols

α	Taylor number $((a^2\omega)/4\nu)^{1/2}$
ε	ratio of characteristic lengths (a/R_0)
π	constant
ν	kinematic viscosity ($m^2 s^{-1}$)
ω	angular velocity ($rad s^{-1}$)
∞	reference value
ψ	Thiele moduli ($C_\infty^{(i_j-1)} S_{ij} K_j a 2/D$)

1. Introduction

Radial flow reactors (Fig. 1) have shown some promise for electroorganic synthesis applications [1–4] but to date the work has been almost exclusively experimental. Little is therefore known about the specific importance of design parameters and scale-up of these reactors. This work describes the first attempt to model the three radial flow reactors for an electroorganic synthesis scheme. Problems in scale-up are identified and two strategies commented on. The interplay of system parameters on reactor scale-up are elucidated.

This detailed electrochemical reactor model was developed [5] and its performance compared to previous models developed by White *et al.* [6] and Nguyen *et al.* [7] for copper winning from an HCl solution. For the simplified reaction scheme therein, this model performed in a comparable if not superior manner. A number of mathematical schemes were employed (finite differences, orthogonal collocation, multi-zone collocation, quasi-linearization) and for a complete

0021-891X/89 $03.00 + .12 © 1989 Chapman and Hall Ltd.

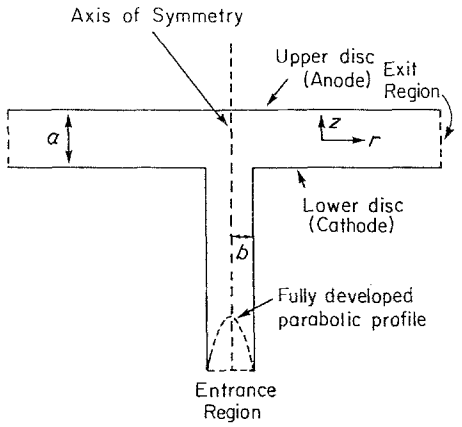

Fig. 1. Radial flow geometry.

description one is referred to Ref. [5]. The model is general for any number of elementary homogeneous reactions and up to four electrode reactions.

2. Methoxylation of furan

Due to increasing interest in electrosynthesis, the model is applied to an electroorganic reaction scheme. The methoxylation of furan is selected as the reaction scheme to analyze for a number of reasons. (1) Experimental studies have been performed [8] which, even if not providing intrinsic information, comment on general kinetic relationships and general parameter ranges. (2) It exhibits a competing reaction pathway, likely to be influenced by the local mixing conditions of the reactors employed. (3) As far as electroorganic syntheses are concerned the system is simple, involving approximately ten components and five reactions – three homogeneous and two electron-transfer reactions. (4) A strong interplay between electrochemical and chemical steps is evident. Bromine, being absent in the feed, is required for furan bromination which leads to product formation. Bromine is generated electrochemically and therefore electrochemical – chemical reaction dependence is paramount. (5) The process has industrial significance, the product, 2,5-dimethoxyfuran, being used in Nylon 4 manufacture.

This system therefore possesses some key components which make it a good candidate for modeling. Subsequent sections describe the methodology used.

2.1. *Chemical reactions*

The reactions involved, in a simplified form are:

Homogeneously

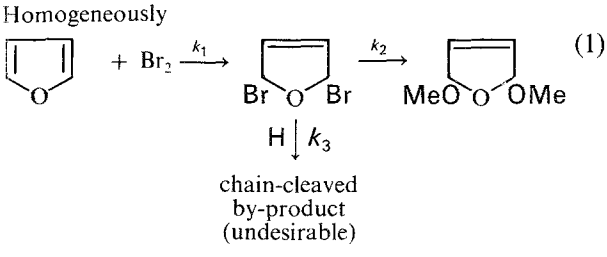

(1)

Electrodes

$$\text{Cathode: } NH_4^+ + e^- \longrightarrow NH_3 + 0.5\,H_2$$
$$\text{Anode: } Br^- \longrightarrow 0.5Br_2 + e^- \qquad (2)$$

The initial bromination, followed by a competitive mechanism, provides a representative description but the actual route may be much more complex. However, due to the lack of available intrinsic kinetic information, inclusion of a more complex reaction system is unjustified at present.

Kinetic information, pertaining to the reaction scheme involved in this system, can at best be inferred based on some qualitative guidelines and qualitative data on similar compounds (see Refs [9–11]). The bromination of furan was estimated at $291\,mol^{-1}s^{-1}$. Jansson *et al.* [11] interpret the methoxylation step as being very fast and the rate was set as 50 times that of the bromination. The reaction rate of the competing reaction, which leads to the chain-cleaved by-product, was set to a value which would provide selectivities of about 80% (approximate selectivities observed experimentally). Some initial runs were then made to check for consistency. It became apparent that not all the bromine was being reacted to form intermediate. Jansson and Tomov [8] concluded that chemical rates were at least as fast as electrochemical rates, since no bromine was observed in the effluent, and therefore the reaction rate of the first step was increased to $10^4\,l\,mol^{-1}s^{-1}$. The subsequent reaction rates were then increased to $5 \times 10^5\,l\,mol^{-1}s^{-1}$ and $301\,mol^{-1}s^{-1}$ for the desired and undesired steps, respectively. Employing these rates, bromine-normalized concentrations were always less than 10^{-5}, whereas with the previous homogeneous rates they were sometimes as high as 0.005.

Two other simplifying assumptions were made. The first was that the methoxylation step was treated as zero order with respect to methanol. This is a good assumption since the methanol concentration is approximately two orders of magnitude larger than that of the electroactive species. Secondly, it was assumed that the NH_4^+ ion was completely stable and does not dissociate; this serves to reduce the number of considered components by one. Despite the simplifications, this reaction route exhibits characteristics which will provide insight into reactor design and scale-up.

The electrode reactions were treated as reversible, each electrode having only one reaction. As with the homogeneous steps, little kinetic data were available on this system. From existing data [12] it appeared that the proton reduction on graphite may be sluggish and the cathodic reaction exchange current density was estimated as on the order of $10^{-9}\,A\,m^{-2}$. For the anodic reaction, even less information was available. An exchange current density as tabulated in Parsons [12] (Table 97 in that reference) for bromine generation from a potassium bromide solution was $32\,A\,m^{-2}$. Therefore representing the cathodic rate as sluggish compared to the anodic rate seems to be a consistent approach. Comparing initial applied vol-

Table 1. Kinetic and thermodynamic data

Reaction	i_0 ($A\,m^{-2}$)	$V_{standard}$ (V)	α (*transfer coeff.*)
Cathode	2×10^{-17}	0.000	0.50
Anode	1×10^{-04}	0.837	0.50

Homogeneous reactions

Reaction	*Rate constant*	*Reaction order*
1	$10\,m^3\,mol^{-1}\,s^{-1}$	2
2	$500\,s^{-1}$	pseudo 1st
3	$0.08\,m^3\,mol^{-1}\,s^{-1}$	2

tages and current densities with the experimental results of Jansson *et al.* [8] the exchange current densities were modified to produce similar results. The kinetic thermodynamic data are summarized in Table 1. Table 2 summarizes the components, feed concentrations and transport properties.

Before proceeding to the description of the model, a brief summary of what was done to translate the physical system into a tractable problem, is provided.

2.2. *Summary of assumptions*

In summary, the following simplifications were invoked in preparing the physical system for mathematical analysis. (1) A model system of eight components was formed out of a solution which could easily consist of upwards of 15 species. It is thought that the species retained will be representative of the system and the interplay between the many transport and reaction processes will be illustrated with the eight-component scheme. (2) A reaction system was incorporated consisting of two electrode reactions and three homogeneous reactions, including a competing reaction pathway. (3) Kinetic data were estimated from the available sources but were eventually altered to provide qualitative consistency with previous experimental results [8].

Other relevant assumptions, inherent in the formulation, will next be discussed with a review of the mathematical development.

3. Mathematical formulation

The assumptions implicit in the model are, in addition to those described in Section 2.2: (1) dilute solution theory holds; (2) double layer effects are insignificant; (3) gas evolution is ignored; (4) Butler–Volmer kinetics are representative; (5) flow field is influenced negligibly by component transport and concentration gradients; (6) interelectrode gap width is much smaller than disc radius; (7) steady-state operation; (8) laminar flow throughout; (9) isothermal operation.

With these assumptions, the steady-state mass balance for component i, in cylindrical coordinates, is given by (where the terms multiplied by $\varepsilon^2(a^2/R_0^2)$ have already been dropped)

$$0 = \frac{\Phi_\infty F Z_i u_i}{D_i}\left(\frac{\partial C_i \partial \Phi}{\partial z \partial z} + C_i \frac{\partial^2 \Phi}{\partial z^2}\right) + \frac{\partial^2 C_i}{\partial z^2} - v_r\left(\frac{v_c a^2}{R_0 D_i}\right)\frac{\partial C_i}{\partial r} - v_z\left(\frac{v_c a}{D_i}\right)\frac{\partial C_i}{\partial z} + \frac{a^2}{D_i}\sum_{j=1}^{N_{RXN}} S_{ij} K_j C_\infty^{(i_j - 1)} \prod_{k=1}^{N} C_k^{n_{jk}} \qquad (3)$$

where the dependent and independent variables are now in dimensionless form. For a derivation of Equation 3 the reader is referred to any standard textbook on transport in electrochemical reactors (Ref. [13] for example). Using the following dimensionless groups,

$$Pe_i = \frac{v_c a}{D_i}; \quad \beta_i = \frac{\Phi_\infty F Z_i u_i}{D_i}$$

along with the homogeneous reaction term, Equation 3 describes the mole balance for component i. Regarding the reaction term, where K_j is the rate constant for reaction j, S_{ij} is the stoichiometric coefficient of the ith component in the jth reaction, n_{jk} is the reaction order for component k in reaction j and i_j is the order of the elementary reaction step, one has defined another dimensionless group ($\psi = C_\infty^{(i_j - 1)} S_{ij} K_j a^2/D$). These groups, one for each component in each reaction, are a ratio of characteristic diffusion time divided by characteristic reaction time and are the Thiele moduli of the system which govern the homogeneous reaction rates.

Table 2. Components, concentrations and transport properties

Component	*No.*	*Charge*	*Inlet concentrations* ($mol\,l^{-1}$)		*Diffusivity* ($m^2\,s^{-1} \times 10^9$)
			Low electrolyte	*High electrolyte*	
Furan	1	0	1.507	1.507	1.0[a]
Dibromofuran	2	0	–	–	1.0
Dimethoxyfuran	3	0	–	–	1.0
Br^-	4	−1	0.186	0.371	1.505
Br_2	5	0	–	–	1.0
NH_4^+	6	+1	0.186	0.371	1.395
H_2	7	0	–	–	–
Chain-cleaved product	8	+1	–	–	1.0

[a] These values of $1.0 \times 10^{-9}\,m^2\,s^{-1}$ were arbitrarily set. The model's performance is very insensitive to these diffusivities.

The velocity contributions are provided by the computations described elsewhere [5, 14]; the length of those calculations precludes their description herein. By specifying the dimensionless groups and the boundary conditions, the system can be solved. As for the purely heterogeneous reaction case [5], the potential was resolved using the electroneutrality constraint.

The electrode boundary conditions relate the species flux to the current density according to the expression (for the cathode)

$$N_i = \sum_{j=1}^{N_{RXN}} \frac{S_{ij} i_j}{n_j F} \qquad (4)$$

with the anodic condition being the same but with opposite sign. For a non-reactive component Equation 4 simplifies to $N_i = 0$. Feed concentrations were specified as essential boundary conditions, and since the problem was translated into an initial value problem in radius, no exit end boundary conditions are required. Since the IVP methodology was used herein, the pump cell could not be simulated over a broad range of parameter values, however, scale-up and design information was obtained for the pump cell according to some guidelines recommended by Jansson and Tomov [8]. The performance of the pump cell at scaled-up conditions will be detailed in the next section of this paper.

The solution procedure used orthogonal collocation in the Z coordinate and an implicit integration scheme in radius. Quasi-linearization was used which lent considerable stability to the non-linear problem. Initially, Picard-type iteration was used and homogeneous rates had to be low in order to retain numerical stability. With quasi-linearization the homogeneous terms retained stability over a broad range of reaction rates (over 8 orders of magnitude).

Having specified the physical constants, the system geometry, the kinetic constants and the applied cell voltage, the performance of four cell types, the parallel plate electrochemical reactor (PPER), the capillary gap cell, the rotating electrolyzer (RE) and the pump cell (PC), could be simulated for a model electroorganic synthesis. Detailed results for the different cell types, along with an interpretation and a scale-up and design commentry, are provided in the next section.

4. Simulation results

Jansson and Marshall [15] reported mass transfer studies performed in a bipolar electrochemical pump cell. This reactor was then used in a later study [8] of the methoxylation of furan, as mentioned earlier. The simulations performed here are done employing conditions as consistent with the previous experimental studies as possible.

4.1. *Bench-scale results*

To quantify the performance of the radial flow electrochemical cells, it was thought advantageous to compare them to the more conventional PPER. The results obtained for that reactor follow.

Table 3. PPER performance

Applied voltage (V)	*Furan conversion (%)*	*Selectivity (%)*[a]	*Flow rate ($m^3 s^{-1}$)*
Low electrolyte concentration[b]			
4.0	0.010	93.74	1.083×10^{-5}
4.25	0.030	93.25	1.083×10^{-5}
4.50	0.063	92.12	1.083×10^{-5}
4.75	0.091	91.54	1.083×10^{-5}
4.00	0.100	92.56	1.083×10^{-6}
4.00	0.900	91.82	1.083×10^{-7}
4.00	6.663	91.10	1.083×10^{-8}
4.25	7.988	90.13	1.083×10^{-8}
4.50	8.009	90.06	1.083×10^{-8}
High electrolyte concentration			
4.25	0.060	87.58	1.083×10^{-5}
4.50	0.115	86.15	1.083×10^{-5}
4.75	0.145	80.00	1.083×10^{-5}
5.00	0.147	74.34	1.083×10^{-5}
4.50	15.750	84.23	1.083×10^{-8}

[a] Selectivity defined as 100 × dimethoxy product/(dimethoxy product + by-product).
[b] Low and high electrolyte concentrations were 0.186 and 0.371 gmol l^{-1} NH_4Br, respectively.

4.1.1. Parallel plate electrochemical reactor. Retaining the same flow rate and gap width as Jansson and Tomov [8] for the pump cell, a PPER was modeled using a square configuration; the electrodes were square with an area of 25.13 cm^2.

Runs were done at 4.5 V (Jansson and Tomov used 5.0 and 7.0 V per gap) and discretization requirements determined. The optimal discretization scheme used 9 collocation points and 25 radial integration steps. This provided a discretization error of only 2% but provided a fourfold economization in CPU time compared to the finest discretization scheme [13, 40]. Almost all runs were then performed with the 9/25 discretization. Table 3 summarizes the series of computations performed for the PPER cell. Performance can be examined as a function of three independent parameters: changing inlet feed concentration, changing flow rate and different applied voltages. From inlet to exit, fully developed flow was assumed in these calculations: parabolic parallel velocities and zero perpendicular velocities. The overall reactor performance is rather complex due to the coupling of all the phenomena. For a detailed discussion of the coupling involved in these reactions, the reader is referred to Ref. [5].

General trends, evident from Table 3 are: (1) conversion of furan per pass increases with increasing applied voltage; (2) selectivity decreases with increasing applied voltage; (3) the reactor is mass transfer limited at the higher voltages; (4) furan conversion is higher with higher electrolyte concentration and lower flow rate, although space time yield would be less; (5) selectivity decreases with decreasing flow rate, as with increasing electrolyte concentration.

Compared to experiment, the simulated current densities were of the same order for the 5.0 V applied (about 2000 A m^{-2} herein compared to 2800 A m^{-2})

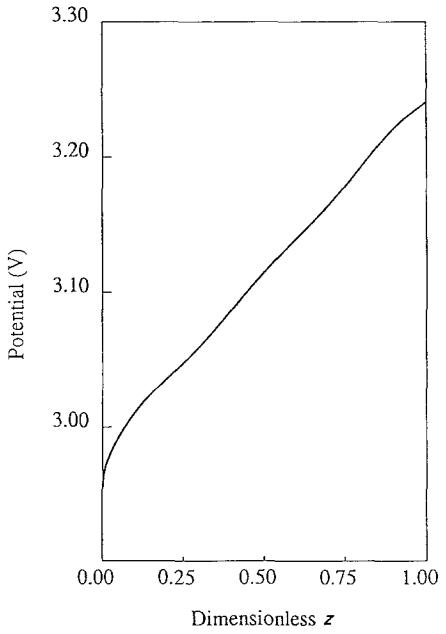

Fig. 2. Parallel plate reactor solution at 5.0 $V_{applied}$. Electrostatic potential vs axial distance. Gap = 0.76 mm and flow rate = 1.08 × 10^{-5} $m^3 s^{-1}$. X = 1.00 (dimensionless distance).

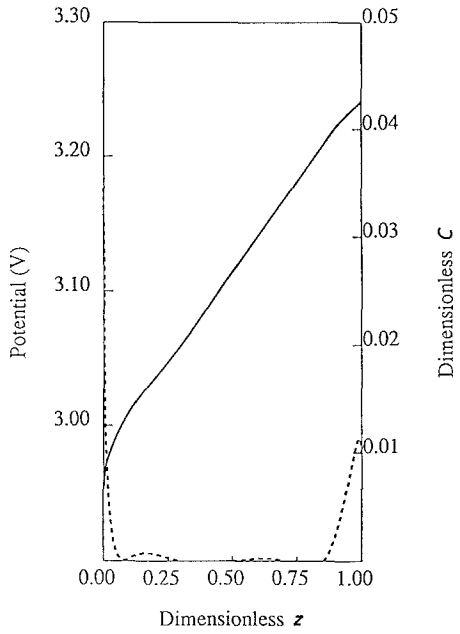

Fig. 3. Parallel plate reactor solution at 5.0 $V_{applied}$. Φ and C vs axial distance. Gap = 0.76 mm and flow rate = 1.08 × 10^{-5} $m^3 s^{-1}$. X = 1.00. (——) potential (V); (– – –) by-product.

but there was no rotation in this cell [16, 17]. For 5.0 V applied, almost half is consumed by cathodic overpotential, activation overpotential being the largest component due to the sluggish exchange current density. The central portion compares to within 5% of obeying Ohms law, which it should, when concentration gradients are minimal. From an examination of the concentration profiles, product is formed only in the anolyte, since bromine is anodically produced and since the Thiele moduli are high (10^7). The molecular bromine is entirely consumed and almost all the dibromofuran intermediate is converted, trends which are consistent with experiment.

Figures 2 and 3 present the potential profile for PPER at the reactor exit. The cathodic overpotential at the exit is almost 3.0 V (60% of total applied voltage) due to the additional mass transfer limitations. The electric field near the cathode is also very high (1669 V cm^{-1}) as required to provide the current density (1344 A m^{-2}). At the inlet the cathodic and anodic E-fields were comparable but differ by a factor of 7 at the exit due to mass transfer effects. One other point of interest is brought out in Fig. 3. It was assumed that the chain-cleaved by-product was charged but not faradaically active. Therefore due to the presence of the very high electric field at the cathode, a considerable concentration gradient must exist. Thus, although the majority of the by-product is produced in the anode region, there is significant cross-gap communication due to the electric fields. In practice this may be deleterious from a current efficiency perspective especially if the by-product were readily reduced. A lack of knowledge regarding this component precludes any further interpretation.

Figure 4 presents the current density plot for the PPER at different voltages. Table 3 shows that the cell is reactant limited, in both the 4.5 and 5.0 V cases, at the reactor exit. Figure 4 also includes the current density profiles at applied voltages of 4.25 and 4.5 V. They are much more uniform since reactant concentrations are less depleted that at the higher voltages.

4.1.2. Capillary gap cell. Runs similar to those of the PPER were then performed for the CG cell. This reactor was modeled with the same dimensions as the experimental pump cell of Jansson and Tomov.

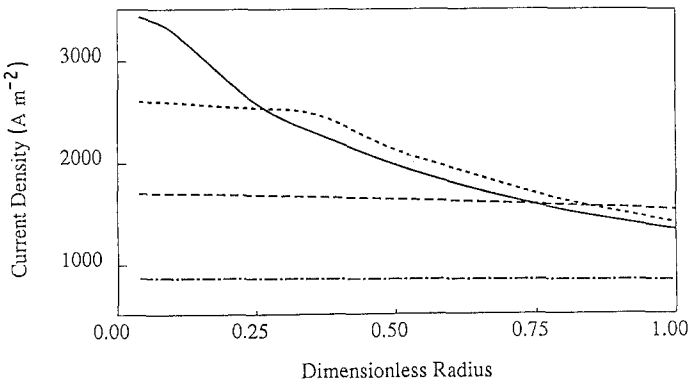

Fig. 4. Parallel plate reactor solutions at 4 voltages. Current density vs dimensionless distance. Gap = 0.76 mm and flow rate = 1.08 × 10^{-5} $m^3 s^{-1}$. (——) $V_{applied}$ = 5.00 V; (– – –) $V_{applied}$ = 4.75 V; (— — —) $V_{applied}$ = 4.50 V; (–·–·–) $V_{applied}$ = 4.25 V.

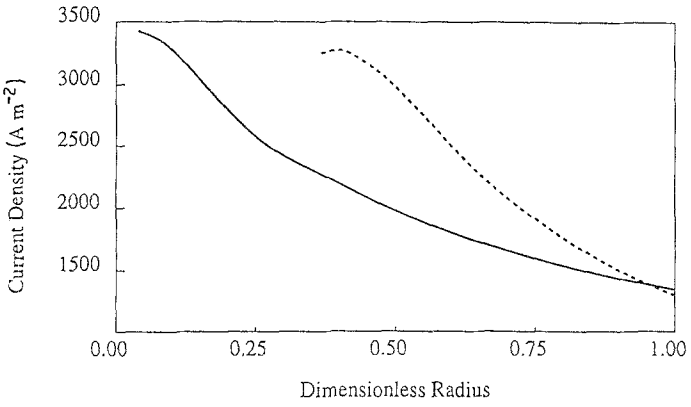

Fig. 5. PPER and CG solutions at 5.0 $V_{applied}$. Current density vs dimensionless distance. Gap = 0.76 mm and flow rate = 1.08 × 10^{-5} $m^3 s^{-1}$. (——) PPER solution (– – –) CG solution.

According to the finite element calculations [5, 14], severe entry effects were not evident in the flow field and therefore a fully developed assumption was made.

Conversion and selectivity were computed with changing applied voltages, flow rates and feed compositions. The same trends as for the PPER were noted in this cell, but the selectivity and furan conversions were slightly higher in the CG than the PPER. Table 4 reports the results for this series of computer runs.

Figure 5 shows the current density profile for the CG at 5.0 V, along with that of the PPER at the same conditions. The PPER current density was higher initially since the PPER inlet velocities were higher (PPER inlet flow area was smaller than the CG). Overall performance however, slightly favored the radial cell as Tables 3 and 4 indicate.

4.1.3. Rotating electrolyzer. In the experimental pump cell of Jansson and Tomov [8], a rotational Reynolds number (Re_θ) of 2.63 × 10^5 was used, corresponding to a rotational speed of 2790 rpm. This rotational speed was used for the rotating electrolyzer simulation. The flow field was computed using the GFEM program [5, 14] and the rv_r asymptotes examined. Essentially fully developed flow was indicated after about 13.5 mm. This is consistent with previous results [5, 14] where it was shown that co-rotational electrodes have a stabilizing influence on flow field.

Figure 6 presents the fully developed radial velocity profile at 25 mm; these conditions provided a Taylor number of 6.5 and therefore well-formed radial velocity jets are present. Runs were then performed, varying flow rate, applied voltage and feed electrolyte concentration as summarized in Table 5. The trends were similar to the other two cells with the exception of selectivity. The REL exhibited higher selectivities and they were essentially unchanged with applied voltage. The conversions were higher due to the convective influences in the reactor.

The high electric fields are again present in the REL but the two electrodes show E-fields of comparable magnitude both at inlet and exit. The enhanced mass transfer was clearly evident. Figure 7 shows the current density distribution for the three cells. The high exit-end current density requires the migrational flux to play a large role at the anode. Since much less of the

Table 4. Capillary gap cell performance

Applied voltage (V)	*Furan conversion (%)*	*Selectivity (%)*	*Flow rate ($m^3 s^{-1}$)*
Low electrolyte concentration			
4.00	0.011	93.84	1.083 × 10^{-5}
4.25	0.029	93.27	1.083 × 10^{-5}
4.50	0.052	92.47	1.083 × 10^{-5}
4.75	0.070	88.11	1.083 × 10^{-5}
4.00	0.097	92.67	1.083 × 10^{-6}
4.00	0.842	91.96	1.083 × 10^{-7}
4.00	5.977	91.38	1.083 × 10^{-8}
4.25	8.394	90.59	1.083 × 10^{-8}
4.50	8.545	90.38	1.083 × 10^{-8}
High electrolyte concentration			
4.00	11.146	85.78	1.083 × 10^{-8}
4.25	16.654	84.85	1.083 × 10^{-8}
4.25	0.062	87.85	1.083 × 10^{-5}
4.50	0.103	87.48	1.083 × 10^{-5}
4.75	0.141	83.05	1.083 × 10^{-5}
5.00	0.164	76.71	1.083 × 10^{-5}

Nomenclature is the same as in Table 3.

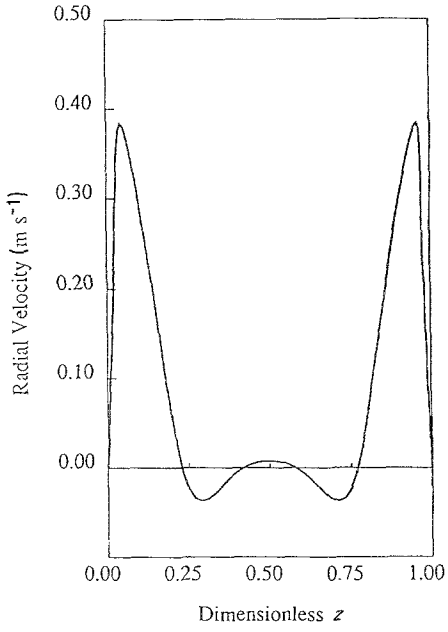

Fig. 6. Rotating electrolyzer solution at α = 6.5. Radial velocity vs axial distance at 2790 rpm. Gap = 0.76 mm and flow rate = 1.08 × 10^{-5} $m^3 s^{-1}$. R_{in} = 10.0 mm; R_{out} = 30.0 mm.

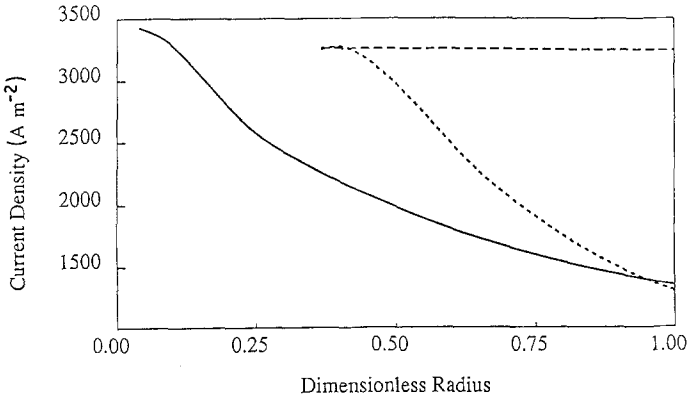

Fig. 7. PPER, CG and REL solutions at 5.0 $V_{applied}$. Current density vs dimensionless distance. Gap = 0.76 mm and flow rate = 1.08×10^{-5} m^3 s^{-1}. (——) PPER solution; (· · · ·) CG solution; (— — —) REL at 2790 rpm.

applied voltage is consumed as cathodic concentration overpotential, that voltage is available to supply the anodic migrational fluxes. The average current density in the REL was 3250 A m^{-2}, whereas the experimental pump cell of Jansson and Tomov registered about 2800 A m^{-2} at these conditions; this would tend to confirm that the kinetics specified in the model are of a reasonable order of magnitude.

It should be noted at this point that the bench-scale pump cell was not simulated due to numerical instabilities caused by the strong reverse flows and large axial velocities. A full 2-D simulation was attempted using a hybrid of collocation and finite difference techniques but convergence was never obtained. Similar problems were not encountered with the large-scale pump cell (to be described later) due to its less severe velocity profiles.

4.1.4. Comparison of bench-scale results. The first trend observed was that furan conversion increased with applied voltage. Since the chemical rate is at least as high as the electrochemical rate [8], this must be the case for an electrochemically mediated reaction system. The only exception to this is when the reactor becomes mass transport limited (NH_4^+). Under these conditions, increased voltage provides no further furan conversion since anodic production is limited by charge conservation ($\nabla \cdot i = 0$) and the cathodic reaction is limited by NH_4^+ ion transport. Therefore the REL, due to its improved convection, provides much higher current densities and concomitant furan conversions compared to the PPER and the CG. From Tables 3, 4 and 5, the high electrolyte runs at 4.5, 4.75 and 5.0 V applied are definitive in terms of mass transport effects. At 4.5 V the three reactors show conversions over 0.10%. At 4.75 V, the three conversions are 0.145, 0.141 and 0.155% for the PPER, CG and REL, the REL being the superior reactor due to its flow field. At 5.0 V the results are more conclusive (0.47, 0.164, 0.206%). Clearly the stationary cells are more mass transport limited than the REL.

Table 5. Rotating electrolyzer performance

Applied voltage (V)	*Furan conversion (%)*	*Selectivity (%)*	*Flow rate ($m^3 s^{-1}$)*
Low electrolyte concentration			
4.25	0.030	94.39	1.080×10^{-5}
4.50	0.057	94.38	1.080×10^{-5}
4.75	0.082	94.37	1.080×10^{-5}
5.00	0.108	94.37	1.080×10^{-5}
4.25	10.165	90.75	1.070×10^{-8}
4.50	10.170	90.21	1.070×10^{-8}
High electrolyte concentration			
4.00	0.016	89.40	1.080×10^{-5}
4.25	0.052	89.40	1.080×10^{-5}
4.50	0.103	89.39	1.080×10^{-5}
4.75	0.155	89.39	1.080×10^{-5}
5.00	0.206	89.39	1.080×10^{-5}
4.00	1.515	87.17	1.080×10^{-7}
4.25	4.725	85.82	1.080×10^{-7}
4.00	11.344	86.09	1.070×10^{-8}
4.25	19.390	84.92	1.070×10^{-8}
4.50	20.177	84.21	1.070×10^{-8}

The furan conversion is higher for higher electrolyte concentrations in the feed. At lower flow rates the conversions are higher, since less is available to react with the electrode products but mass transport limitations arise at lower applied voltages (compared to the higher flow rates). Although conversions are higher at lower flow rates, space–time yields are less. To maintain constant space–time yields, the conversion would have to increase by a factor equal to flow rate reduction; the changes are of similar orders but conversion never increases as much as flow rate is reduced due to transport effects. Selectivities decrease with increasing voltage, increasing electrolyte concentration and decreasing flow rate. This is very evident for the stationary cells although the REL shows almost constant selectivity. These observations may all be described in terms of mass transfer limitations. As mass transfer decreases the ammonium ion concentration at the cathode approaches zero. By electroneutrality, the bromide ion concentration is also fairly low (not exactly equal to NH_4^+ since some chain cleavage by-product is present at the cathode). The bromide ion concentration at the anode remains fairly high (due to reaction recycling) which in turn, by the electroneutrality constraint, maintains a fairly high NH_4^+ ion concentration in the anolyte layer. It is the reaction of the cation and the dibromo intermediate that reduces selectivity.

The simulated results agree with those of Jansson and Tomov with the exception of one. The simulation predicts better energy efficiency at lower concen-

tration while the experiment indicates the opposite. This could be related to the fact that the proton released from the dimethoxy product reaction was not included as a separate component. It is possible that only the proton being released, upon the formation of the dimethoxy product, produces chain cleavage and not the cation present initially (NH_4^+). This might alter the global response of the process and thus explain the discrepancy. In light of the many coupled phenomena however, nothing more can be concluded as to the cause of this discrepancy.

Making a comparison with the experimental results, beyond a qualitative perspective, is not possible at this time. The experimental apparatus was a continuous closed system, the electrolytic solution being recycled many times (approximately 30 000 passes). Future work will be to extend the model to include the multiple pass option, but such will be developed only after some of the physical constants, especially the kinetics, have been ascertained.

The next step taken was to investigate the reactor performance on a larger scale. Jansson and Tomov mentioned that by scaling up the factor of 10, in terms of disc size, retaining the same Re_θ, a very efficient reactor of industrial size could be developed. Retaining Re_θ as 2.63×10^5, for a change in disc size from 30 to 300 mm, allows a decrease in rpm from 2790 to 28. To examine possible scale-up methodologies, the larger reactors were modeled with the exception of the PPER.

4.2. *Industrial scale reactor results*

The reactors modeled herein were scaled-up maintaining a constant Re_θ which has seemed to be the most consistent design strategy in the past. Accordingly, Jansson and Tomov stated that their bench-top cell could be expanded by an order of magnitude, and by maintaining the same gap width, flow rate and Re_θ, similar performance would be achieved.

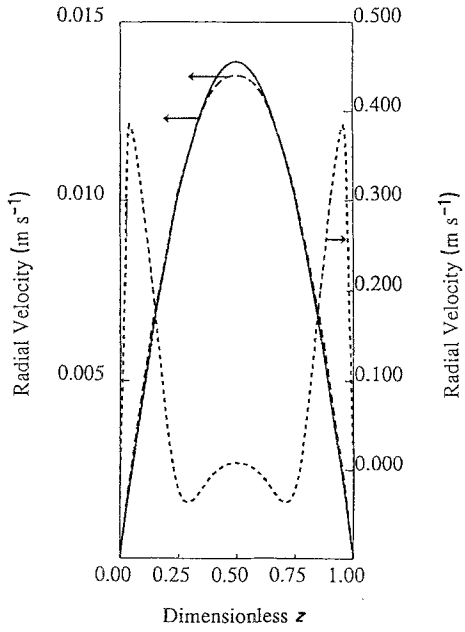

Fig. 8. CG and REL comparisons. Radial velocity changes between small and large cells. Gap = 0.76 mm and flow rate = 1.08×10^{-5} m^{3}s^{-1}. (——) large CG, (· · ·) small REL and (– – –) large REL solutions.

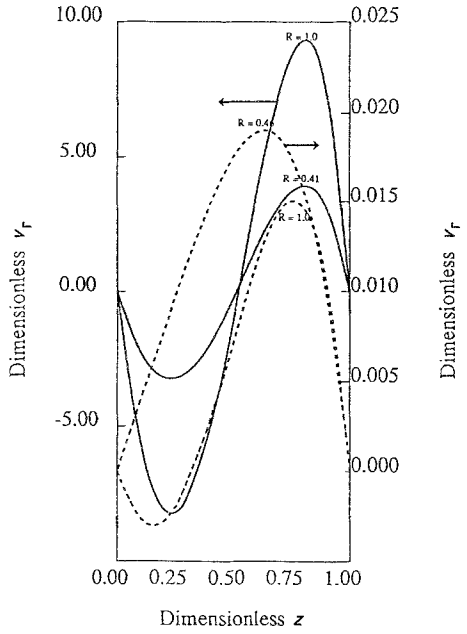

Fig. 9. Radial velocity comparisons between small and large cells. Gap = 0.76 mm and flow rate = 1.08×10^{-5} m^{3}s^{-1}. V_r comparisons; $V_c = 1.31$ m s^{-1}. (——) 2790 rpm (small); (– – –) 28 rpm (larger).

This approach was then followed in specifying the reactors to simulate. The large scale parameters are: inner and outer electrode radii, 10 and 300 mm; gap width, 0.76 mm; flow rate (m^{3}s^{-1}), 1.083×10^{-5} (0.651 min^{-1}). These were input to the simulator retaining all other parameters as they were in the bench-scale computations.

With the larger radius, fully developed flow was definitely a good assumption (over 99% of the reactor area would be in the fully developed region). The CG cell velocity profile did not change. The large-scale REL flow field was calculated with the GFEM program [5, 14] and its velocities changed drastically with scale-up. Although Re_θ was maintained in the scale-up, maintaining a constant gap width resulted in an order of magnitude decrease in Taylor number. Figure 8 presents a comparison of the v_r profiles for the CG and REL large cells, along with the REL radial velocity profile present in the bench scale (where the Taylor number was 6.5 compared to 0.65). Similarly, the change in the pump cell velocities was as marked as for the REL. Figure 9 presents the radial and axial velocities present in the large-scale PC with the bench-scale radial velocities superimposed. There was a significant difference in radial velocities and the axial velocities were four orders of magnitude larger in the smaller cell ($\alpha = 6.5$) than in the larger cell. Therefore if Re_θ is maintained but α altered, the flow field may be very different.

Table 6 summarizes the results for the three cells described. The velocity profiles being so similar for the CG and REL, it is to be expected that they perform similarly. Figure 10 presents the current density distri-

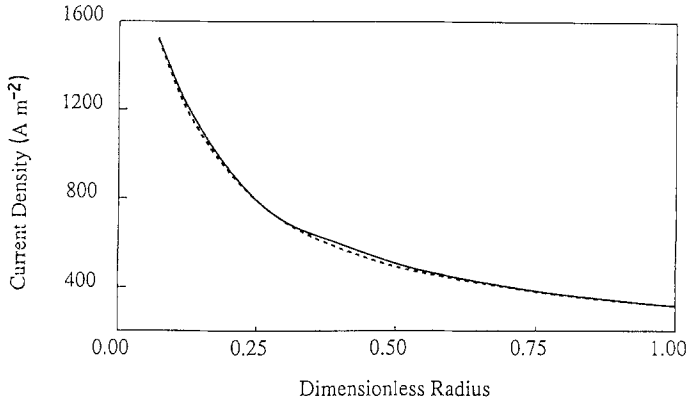

Fig. 10. Large-scale CG and REL solutions at 4.5 $V_{applied}$. Current density vs dimensionless radius. Gap = 0.76 mm and flow rate = $1.08 \times 10^{-5} m^3 s^{-1}$. (——) CG cell; (– – –) REL at 28 rpm.

butions. At this juncture Fig. 7 can be compared. There (for the smaller cells) the difference in cell performance was large, but for these large cells there is no difference between the performance of the capillary gap cell and the rotating electrolyzer. Hence, other scaling criteria must be involved in addition to Re_θ.

Conversions per pass are much higher in the larger cells due to the increase in electrode area. Conversions are approximately two orders of magnitude higher, electrode area being larger by a factor of 112. Comparison may be made between small and large scales by juxtaposing their potential and concentration profiles. For example, Fig. 11 shows a plot of cathodic NH_4^+ concentration for the small and large CG cells. At the exit, it is obvious that the large cell is becoming mass transport limited, thus decreasing conversion below the expected two orders of magnitude. Comparing the lower voltages, for the CG cell, the conversion increase is more in line with the electrode area change. Differences in potential profiles, from the small to the large scale, can be attributed to the extent of conversion and accompanying transport effects.

Altering flow rate and voltage had the same influence at the large scale as in the smaller reactors so different compositions were not computed. Performance may be estimated based on the runs performed at the smaller size.

Table 6. Large scale reactor performance

Applied voltage (V)	*Furan conversion (%)*	*Selectivity (%)*	*Flow rate ($m^3 s^{-1}$)*
Capillary gap cell			
4.00	1.72	86.21	1.083×10^{-5}
4.25	3.26	84.19	1.083×10^{-5}
4.50	3.88	82.86	1.083×10^{-5}
4.00	2.79	85.88	5.417×10^{-6}
4.25	5.66	83.99	5.417×10^{-6}
Rotating electrolyzer, 28 rpm			
4.00	1.49	86.27	1.083×10^{-5}
4.25	3.30	84.19	1.083×10^{-5}
4.50	3.78	82.93	1.083×10^{-5}
4.25	5.71	84.00	5.417×10^{-6}
Pump cell, 28 rpm, cathode spinning			
4.00	7.21	86.20	1.083×10^{-5}
4.25	14.58	84.38	1.083×10^{-5}
4.50	13.53	83.74	1.083×10^{-5}
Pump cell, 28 rpm, anode spinning			
4.00	1.08	86.69	1.083×10^{-5}
4.25	1.94	85.27	1.083×10^{-5}
4.50	2.01	76.90	1.083×10^{-5}

The last two divisions of Table 6 refer to the large-scale pump cell. This larger PC has more 'uniform' radial velocities than the bench-scale cell and therefore could be simulated. Two different modes were analyzed: one where the cathode was spinning and other where the anode was spinning.

With the cathode spinning, there is a net axial flow towards it. The NH_4^+ transport was the limiting factor and therefore a net axial velocity towards the cathode should enhance the performance. Table 6 substantiates this. Conversion was more than four times higher in the PC than in the other two reactors.

Figure 12 illustrates the effect of rotation on the current density profile. The capillary gap cell and rotating electrolyzer have monotonously decreasing current density with radius. The pump cell however, has a minimum at about $r = 0.381$ (239 A m^{-2}), after which current density increases steadily towards the periphery (301 A m^{-2}). Coupling this current density with the increasing area results in the better performance noted in Table 6.

With the anode spinning, there is net flow away from the cathode; mass transport limitations should dominate at lower voltages and performance might be worse. Table 6 shows this. Mass transport becomes restrictive at about 4.25 V and 4.50 V, and conversion is about one-seventh of that when the cathode is spinning. Performance under these conditions is much worse than for the stationary cell.

5. Further interpretation and summary

In the bench-scale simulations the parallel plate and capillary gap cells performed approximately the same, the CG cell being marginally superior for the synthesis examined. The REL at 2790 rpm was much superior to the two stationary cells both in terms of furan conversion per pass and selectivity. Because of the form of the pump cell velocity profiles, the bench scale PCs could not be simulated.

The radial reactors were scaled up (a factor of 10) based on maintaining the same rotational Reynolds number; the rotational speed of the PC and REL was

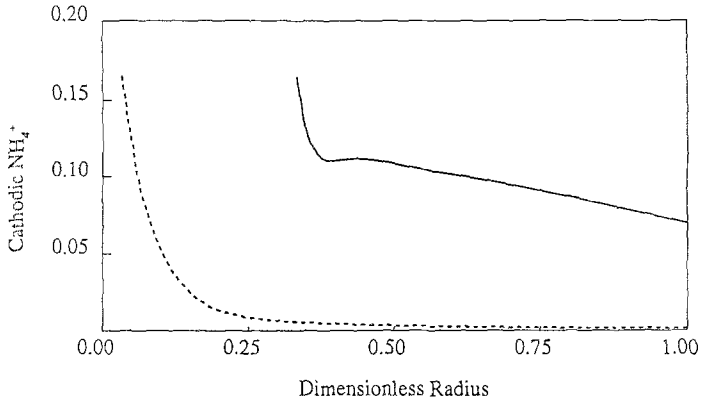

Fig. 11. Small and large capillary cells at 4.5 $V_{applied}$. Cathodic NH_4^+ concentration. Gap = 0.76 mm and flow rate = 1.08 × 10^{-5} $m^3 s^{-1}$. (——) Small CG; (– – –) large CG.

reduced to 28 rpm, the Taylor number being reduced from 6.5 to 0.65. Under these conditions, the difference between the CG and REL velocities is minimal and the performance is essentially the same. It was not the same at the bench scale and hence, rotational Reynolds number is not the only parameter which must be considered when scaling-up the electroorganic process of this type. It is thought that many variables must be considered when attempting to scale-up. It is evident that Taylor number is the more important flow field parameter, it being $a/2\,(\omega/\nu)^{1/2}$. It is independent of cell radius and therefore for decreased rpm in cells the gap width must increase to maintain the Taylor number. Increasing gap width however, increases residence time for a given flow rate, and also increases the *IR* drop thus altering the whole performance of the reactor. Thus, scale-up will probably involve modification of the radius, gap width, flow rate and/or concentration in addition to applied voltage.

This scale-up methodology was then applied to the REL. The disc radius was altered while maintaining constant α, Re_θ and residence time at the same feed composition. It is expected that applied voltage will have to be increased slightly, which can hopefully be estimated by Ohm's law based on the bench-scale current densities.

Table 7 reports the results of the scale-up for a factor of 10 increase in electrode area. Maintaining the above parameters constant (α, Re_θ, τ, C_{feed}) the only change in performance should be due to increased *IR* drop across the larger gap (3.0 times larger — 2.28 vs 0.76 mm). Figure 13 presents the radial velocity profiles for the 0.76 and 2.28 mm gaps; each has a Taylor number of 6.5. The dimensionless form of these is very close, indicating that Taylor number completely determines the axial shape of the radial velocity profile; it was seen before to be very insensitive to flow rate, after the entry region [5, 14]. Therefore, as mentioned elsewhere [5, 14], once the flow field is computed for one Taylor number, the radial velocities can be accurately calculated for the desired flow rate and gap width, as long as α is maintained.

For the 4.00 V (small reactor) and 4.50 V (larger reactor) runs, their conversions, space-time yields and selectivities are very similar. The average current density for the small cell was 250 A m^{-2} (essentially constant) whereas that of the larger cell was 670 A m^{-2}. The larger area was 10 times that of the smaller and therefore approximately 26.8 times as much electrodic reaction occurred in the large cell, compared to the bench scale. The flow rate, in the large reactor, was 30.0 times that of the small reactor however, and therefore one would expect a decrease of 0.893 (26.8/30.0) in conversion. The computed conversions were different by a factor of 0.875.

Next, the applied voltage was altered to account for the change in the interelectrode gap. The average conductivity of the bulk solution was about 4.0 $\Omega^{-1} m^{-1}$, which for the small cell corresponds to an overall electric field of about 62 V m^{-1}. The *IR* drop would therefore be approximately 0.00076 m × 62 V m^{-1} or 0.047 V. Therefore the expected *IR* drop should be about 0.14 V for the larger gap. The applied voltage was then increased to 4.094 V and the con-

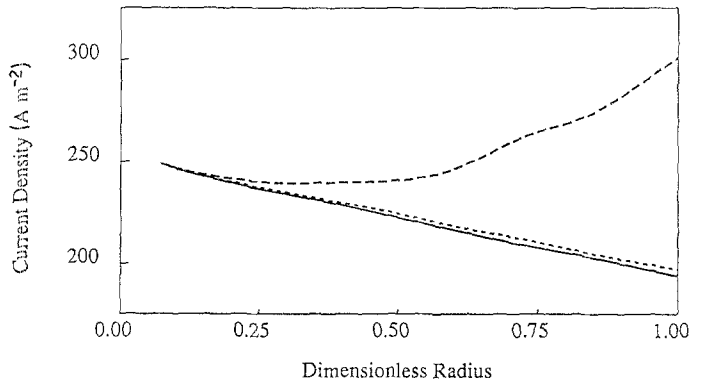

Fig. 12. CG, REL and PC solutions at 4.0 $V_{applied}$. Current density vs dimensionless radius. Gap = 0.76 mm and flow rate = 1.08 × 10^{-5} $m^3 s^{-1}$. (——) CG cell; (– – –) REL at 28 rpm; (— — —) PC at 28 rpm.

Table 7. Results for scale-up tests, rotating electrolyzer

Applied voltage (V)		*Furan conversion (%)*		*Space–time yield ($mol\,m^3\,s^{-1}$)*		*Selectivity (%)*	
4.00	4.50	0.016	0.014[a]	1.32	1.24	89.40	89.47
4.25	4.094	0.052	0.004	4.39	0.44	89.40	89.40
4.50	4.75	0.103	0.018	8.59	1.75	89.39	89.48
4.75	5.00	0.155	0.027	13.04	2.23	89.39	89.50
5.00	5.11	0.206	0.028	17.28	2.42	89.39	89.47
	5.50		0.034		3.23		89.49
	6.00		0.044		3.83		89.50
	6.50		0.049		4.28		89.51
	7.00		0.054		4.60		89.54

	Cell parameters	
	Small	*Large*
Inside radius (m)	0.010	0.010
Outside radius (m)	0.030	0.090
Gap width (mm)	0.760	2.280
Electrode area (cm^2)	25.13	251.3
Flow rate ($m^3\,s^{-1}$)	1.083×10^{-5}	3.258×10^{-4}

[a] Underlined numbers are those of the larger reactor. Maintaining constant τ in the scale-up results in very low conversions due to the 30-fold increase in flow rate. Higher voltages could be applied but at voltages above 8 V stability problems were encountered. Although the per-pass conversions are low, they are converged solutions and round-off errors are negligible.

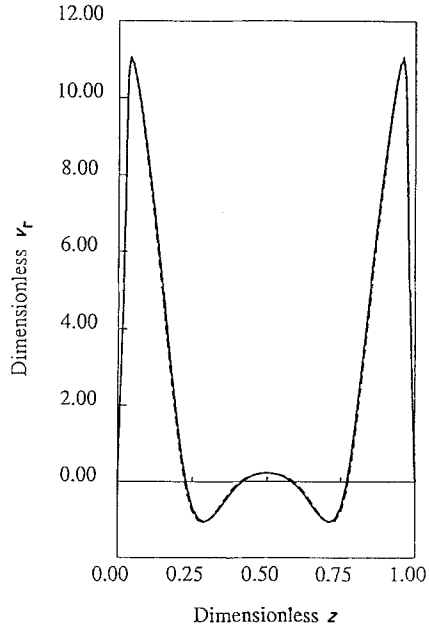

Fig. 13. Rotating electrolyzer solution. Radial velocity comparison. (——) Small REL solution; (– – –) area × 10 REL solution.

versions computed. The average current density was 240 A m^{-2}, comparing very well with the 250 A m^{-2} of the small reactor. Under these conditions, the reactor performance, according to production of dimethoxyfuran, was according to scale-up: the larger cell produced 9.92 times as much (per pass) as the smaller cell.

The 4.45 V run (small reactor) was then analyzed. It exhibited an average current density of about 1630 A m^{-2}. Using the same *IR* methodology as above (the average electric field was 402 V m^{-1}) the cell voltage should be about 5.11 V for the larger cell. In this case the large cell generated only 8.4 times as much product per pass as the smaller cell. If scale-up were done according to Re_θ only, the production factor would be 6.5. An applied voltage of 5.5 V was required for the large reactor to produce 10 times as much as the 4.5 V smaller reactor.

Higher voltages were tried but the deviation became more accentuated. The 5.0 V small reactor had an average current density of about 3260 A m^{-2}. To obtain similar performance in the scaled-up reactor an applied voltage of 6.22 V should suffice. Under these conditions an average current density of 2045 A m^{-2} was attained, the larger reactor producing only 6.5 times as much as the smaller cell.

This behavior can be explained in terms of transport of the ammonium ion. In the smaller cell there was better transport of cation to the cathode for two reasons. The first concerns the physical location of the radial velocity jet. Although the dimensionless form is very similar, between the 0.76 and 2.28 mm gaps, the actual location is a factor of three closer (to the electrodes) in the smaller cell. This could provide greater driving force for diffusion towards the electrode. The second factor pertains to diffusion effects once again but in the sense described elsewhere [5]. There it was shown that the characteristic diffusion time increases as a function of gap width squared. Thus, if transport via diffusion and convection are reduced by increasing gap, then to maintain electrodic reaction rates, migration effects must compensate. If the applied voltage is not large enough to compensate, then reduced performance and deviation from scale-up expectation is inevitable.

Mention should be made concerning the design and scale-up of the pump cell. Compared to the rotating electrolyzer, of which the flow field (v_r and v_z) was determined by the Taylor number only, the pump cell would be at least as difficult to scale since its radial and axial velocities are functions of flow rate as well. Therefore, to maintain scale-up performance, all variables would have to be considered simultaneously. Since the full 2-D simulator developed for the PC was numerically unstable for strong reverse flows, no further commentary can be provided for the pump cell at this time.

The scale-up strategy, suggested for the REL (which is applicable for the capillary gap cell as a subset) is better than basing design only on Re_θ, but at higher applied voltages the suggested technique fails. In light of these findings, maintaining constant Taylor number, τ, C_{feed} and Re_θ does not appear to be a panacea for the woes of scaling. The insight gained here, however, does indicate some further directions in which to look. Further theoretical and experimental work is now progressing in this area.

Acknowledgement

The authors express their appreciation to Monsanto Corporation for their generous funding of this project over the years 1984–1987. They also thank

Hycal Energy Research Ltd for covering the costs of publication.

References

[1] J. Ghoroghchian, R. E. W. Jansson and D. Jones, *J. Appl. Electrochem.* 7 (1977) 437.

[2] J. Ghoroghchian and R. E. W. Jansson, *J. Chem. Tech. Biotech.* **30** (1980) 44.

[3] R. E. W. Jansson and N. R. Tomov, *Electrochim. Acta* **25** (1980) 497.

[4] R. E. W. Jansson, 'Control of Electrochemical Reactions by Cell Design and Mode of Operation', Verlag Chimie, Berlin, (1983) Vol. 94, pp. 33–53.

[5] F. B. Thomas, 'Modeling of laminar radial-flow electrochemical cells'. D.Sc. thesis, Washington University, St Louis, MO, USA, August 1987.

[6] R. E. White, M. Bain and M. Raible, *J. Electrochem. Soc.* **130** (1983) 1037.

[7] T. V. Nguyen, C. W. Walton, R. E. White and J. Van Zee, *J. Electrochem. Soc.* **133** (1986) 81.

[8] R. E. W. Jansson and N. R. Tomov, *Chem. Ind.* (1978) 96.

[9] S. Clementi, F. Genel and G. Marino, *Chem. Commun.* (1967) 498.

[10] P. Linda and G. Marino, *Chem. Commun.* (1967) 499.

[11] R. E. W. Jansson and M. Fleischmann, 'Effect of Cell Design on Selectivity and Conversion in Electro-organic Processes', American Institute of Chemical Engineers Symposium Series, No. 185, Vol. 75, (1979) pp. 2–7.

[12] R. Parsons, 'Handbook of Electrochemical Constants', Butterworths Scientific Publications, London (1959).

[13] J. Newman, 'Electrochemical Systems', Prentice Hall, Englewood Cliffs, New Jersey (1973).

[14] F. B. Thomas, P. A. Ramachandran, M. P. Dudukovic and R. E. W. Jansson, *J. Appl. Electrochem.* **18** (1988) 768.

[15] R. E. W. Jansson and R. J. Marshall, *Chem. Eng.* Nov/Dec. (1976) 769.

[16] G. A. Ashworth and R. E. W. Jansson, *Electrochim. Acta* **22** (1977) 1295.

[17] R. E. W. Jansson and G. A. Ashworth, *Electrochim Acta* **22** (1977) 1301.